THE JOURNAL OF PHYSICAL CHEMISTRY Letters

Letter

pubs.acs.org/JPCL

Determination of Spin Inversion Probability, H-Tunneling Correction, and Regioselectivity in the Two-State Reactivity of Nonheme Iron(IV)-Oxo Complexes

Yoon Hye Kwon,[†,#] Binh Khanh Mai,[‡,#] Yong-Min Lee,[†] Sunder N. Dhuri,[†,¶] Debasish Mandal,[§] Kyung-Bin Cho,*[,†] Yongho Kim,*[,‡] Sason Shaik,*[,§] and Wonwoo Nam*[,†]

[†]Department of Chemistry and Nano Science, Ewha Womans University, Seoul 120-750, Korea

[‡]Department of Applied Chemistry and Institute of Natural Sciences, Kyung Hee University, Gyeonggi-do 446-701, Korea

[¶]Department of Chemistry, Goa University, Goa 403 206, India

[§]Institute of Chemistry and the Lise Meitner-Minerva Center for Computational Quantum Chemistry, The Hebrew University of Jerusalem, 91904 Jerusalem, Israel

Supporting Information

ABSTRACT: We show by experiments that nonheme $Fe^{IV}O$ species react with cyclohexene to yield selective hydrogen atom transfer (HAT) reactions with virtually no C═C epoxidation. Straightforward DFT calculations reveal, however, that C═C epoxidation on the S = 2 state possesses a low-energy barrier and should contribute substantially to the oxidation of cyclohexene by the nonheme $Fe^{IV}O$ species. By modeling the selectivity of this two-site reactivity, we show that an interplay of tunneling and spin inversion probability (SIP) reverses the apparent barriers and prefers exclusive S = 1 HAT over mixed HAT and C═C epoxidation on S = 2. The model enables us to derive a SIP value by combining experimental and theoretical results.

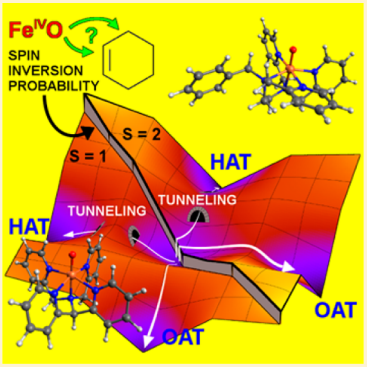

The concept of two-state reactivity (TSR) was formulated for the first time to account for the intriguing reactivity patterns in the oxidation of H_2 and small alkanes by FeO^+.[1,2] This concept was quickly shown to carry over to the oxidation of alkanes by nonheme iron(IV)-oxo complexes,[3−5] such as $[(N4Py)Fe^{IV}(O)]^{2+}$ (**1**) and $[(Bn\text{-}TPEN)Fe^{IV}(O)]^{2+}$ (**2**) complexes (Figure 1).[3,6] In all of these processes, the S = 1 spin state is the ground state of the reactants, but the reactions seemed invariably to be mediated by the S = 2 state due to its significantly lower activation barriers.[7,8] However, the spin inversion probability (SIP), which controls the likelihood of such a crossover, is a product of spin−orbit coupling (SOC) and other variables not easily calculated. It has therefore often, but not always,[9] been neglected, and the spin inversions have been assumed to occur with probability that depends on the initial spin state's energy differences. We present here a case where SIP *cannot* be neglected, and its value is extracted from the combined experimental and theoretical data. As will be seen, this will further enable us to estimate the impact of SOC on selectivity and to do so in a widely applicable manner for two-site and two-state reactions. The case studied here is the oxidation reaction of cyclohexene (CHE-h_{10}) and its fully deuterium-substituted analogue (CHE-d_{10}) by **1** and **2**.

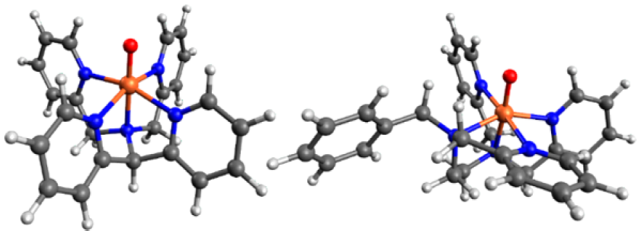

Figure 1. Two catalysts, $[(N4Py)Fe^{IV}(O)]^{2+}$ (**1**, left) and $[(Bn\text{-}TPEN)Fe^{IV}(O)]^{2+}$ (**2**, right), used in this study. N4Py = *N*,*N*-bis(2-pyridylmethyl)-*N*-bis(2-pyridyl)methylamine, Bn-TPEN = *N*-benzyl-*N*,*N*′,*N*′-tris(2-pyridylmethyl)-1,2-diaminoethane.

A second key issue in this work is quantum mechanical tunneling.[10−17] The most ubiquitous room-temperature tunneling has been associated with the observation of large kinetic isotope effects (KIEs) in hydrogen atom transfer (HAT) reactions.[18−20] As we demonstrate here, tunneling renders the S = 1 HAT process energetically accessible at ambient temperature, thus contributing significantly to the selectivity patterns in TSR.[21]

Received: March 12, 2015
Accepted: March 30, 2015

DOI: 10.1021/acs.jpclett.5b00527
J. Phys. Chem. Lett. 2015, 6, 1472−1476

The oxidation of CHE-h_{10} by **1** and **2** was carried out in CH_3CN at 25 °C under an Ar atmosphere. Upon addition of CHE-h_{10} to the solutions of **1** and **2**, the intermediates disappeared completely (Figure 2a for **1** and Supporting Information (SI) Figure S1a for **2**). Pseudo-first-order rate constants k_{obs}, determined by the first-order fitting of the kinetic data for the decay of **1** and **2**, increased linearly with an increase of the CHE-h_{10} concentration (Figure 2b and SI, Figure S1b), giving us second-order rate constants of $4.5(4) \times 10^{-2}$ and $4.5(4) \times 10^{-1}$ M^{-1} s^{-1} for the reactions of **1** and **2** at 25 °C, respectively. Interestingly, when the reactions were carried out with CHE-d_{10}, the second-order rate constants were determined to be $8.2(6) \times 10^{-4}$ and $6.8(6) \times 10^{-3}$ M^{-1} s^{-1} for the reactions of **1** and **2** at 25 °C, respectively (Figure 2b and SI, Figure S1b). From the second-order rate constants, KIEs of 55(5) and 66(5) were obtained for the reactions of **1** and **2**, respectively.

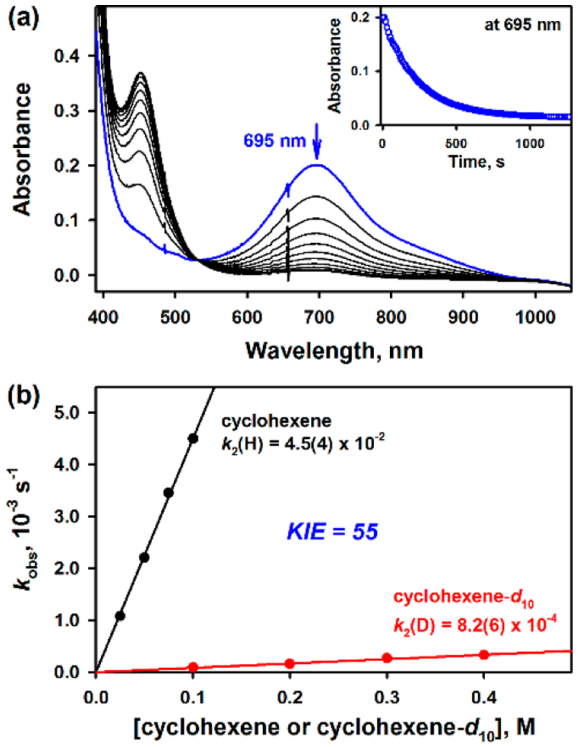

Figure 2. (a) UV−vis spectral changes observed in the reaction of **1** (0.50 mM, blue line) and CHE-h_{10} (1.0×10^2 mM) in CH_3CN at 25 °C. The inset shows the time course monitored at 695 nm. (b) Plots of the first-order rate constant, k_{obs} (s^{-1}), against the concentration of CHE-h_{10} (black) and CHE-d_{10} (red) to determine second-order rate constants, k_2 (M^{-1} s^{-1}), and the KIE value.

Product analysis of the reaction of **1** and CHE-h_{10} revealed the formation of cyclohexen-2-ol (18(2)%) and cyclohexen-2-one (15(2)%) but only a trace amount of CHE oxide (<0.5%) (SI, Table S1).[22−26] The total product yield corresponded to what is expected for a nonrebound mechanism.[27] Similar product distribution was observed in the oxidation of CHE-h_{10} by **2** (SI, Table S1). When ^{18}O-labeled PhIO was used to generate **1** and **2**, the oxygen in the cyclohexen-2-ol product was found to derive from the $Fe^{IV}O$ species (SI, Experimental Section and Figure S2). Further, the iron products formed in the CHE-h_{10} oxidation by **1** and **2** were determined to be iron(III) species (SI, Figure S3), as we have shown in the C−H bond activation of alkanes by **1** and **2**,[27] with similar results also observed by others.[28,29] Upon using CHE-d_{10}, the CHE oxide product increased to 9(2)% with **1** and 8(2)% with **2** coupled to a slight decrease of the other product yields (SI, Table S1).

For comparison, because styrene does not possess allylic C−H bonds, we carried out the oxidation of styrene and deuterated styrene by **1** and **2** (see the text in the SI for details). The KIE values determined here were ∼1 (SI, Figure S4). Product analysis revealed the formation of styrene oxide as the major product (e.g., >80%; SI, Table S1) and the $Fe^{IV}O$ species as the source of the oxygen in the styrene oxide product (SI, Figure S5). In addition, the iron products formed in the styrene oxidation by **1** and **2** were iron(II) species (SI, Figure S3). Also, the enthalpy and entropy values were the same in the reactions of styrene and deuterated styrene by **1**, in contrast to the reactions with CHE-h_{10} and CHE-d_{10}, where the entropy values were different depending on the substrates (SI, Figure S6). These differing results regarding the KIE, product analysis on both organic and inorganic products, and entropy when using styrene vis-à-vis CHE as substrates support the notion that the oxidation of CHE-h_{10} by **1** and **2** occurs via an allylic HAT reaction including tunneling. However, some epoxidation reactions, henceforth denoted oxygen atom transfer (OAT) reactions in the current study, are taking place as well when using CHE-d_{10}.

We now attempt to model this regioselectivity and the large KIE value observed in the HAT reaction of CHE by using density functional theory (DFT) and variational transition state theory (VTST)[30] including multidimensional tunneling calculations. The general idea is that if little or no OAT occurs normally but more OAT occurs upon deuteration, the difference must be attributed to the close energy barriers between HAT and OAT, so close that deuteration can change the preference (akin to metabolic switching in enzymatic reactions).[31] Because only the $S = 2$ spin state has a low enough barrier for the OAT reaction, the amount of OAT products upon deuteration will be indicative of the SIP.

This idea can be analyzed as follows. The total amount of organic products [P_{tot}] can in principle involve HAT and OAT in the two spin states, $S = 1$ and 2, namely

$$[P_{tot}] = [^3P_H] + [^5P_H] + [^3P_O] + [^5P_O] \quad (1)$$

Here, the superscripts 3 and 5 denote the multiplicity, $M = 2S + 1$, of the corresponding reaction path. Hence, eq 1 expresses the total amount of organic products as a sum of products produced by the $S = 1$ and 2 HAT pathways ($[^3P_H] + [^5P_H]$) and their OAT counterparts ($[^3P_O] + [^5P_O]$). The products [^3P_H] and [^5P_H] are of course physically indistinguishable as they are the same organic products (as are [^3P_O] and [^5P_O]), but they are produced by **1** and **2** in the respective spin states.

Table 1 lists the DFT calculated rate-limiting free energy barriers for the four reactions, relative to the same reference point (see the SI, Rate Calculations section and Table S2 for methods). Let us now analyze these data according to the Boltzmann factors. We define the natural SIP as

$$f_{SI}^{\circ} = \frac{e^{-{}^5\Delta G^{VTS(H)}/RT} + e^{-{}^5\Delta G^{VTS(O)}/RT}}{e^{-{}^3\Delta G^{VTS(H)}/RT} + e^{-{}^5\Delta G^{VTS(H)}/RT} + e^{-{}^3\Delta G^{VTS(O)}/RT} + e^{-{}^5\Delta G^{VTS(O)}/RT}} \quad (2)$$

f_{SI}° is hence the combined probability of the high-spin pathway reactions according to the Bolzmann factor. Using the values

DOI: 10.1021/acs.jpclett.5b00527
J. Phys. Chem. Lett. 2015, 6, 1472−1476

Table 1. DFT Energy Barriers in kcal mol^{-1} and Calculated KIE[a]

		$\Delta G^{\ddagger b}$	$+\Delta_{Tun}{}^{c}$	$+\Delta_{Deu}{}^{d}$	KIE[e]
1	$^3\Delta G^{VTS(H)}$	23.59	−2.83	+2.35	53
	$^5\Delta G^{VTS(H)}$	20.35	−0.32	+0.86	4
	$^3\Delta G^{VTS(O)}$	33.12	+0.01	−0.08	0.9
	$^5\Delta G^{VTS(O)}$	20.15	+0.28	−0.02	1
2	$^3\Delta G^{VTS(H)}$	22.08	−2.71	+2.50	68
	$^5\Delta G^{VTS(H)}$	14.40	−0.12	+0.95	5
	$^3\Delta G^{VTS(O)}$	28.72	−0.01	−0.08	0.9
	$^5\Delta G^{VTS(O)}$	15.23	+0.03	−0.02	1

[a]Calculated at the B3LYP/Def2-TZVPP//6-31G(d) level at 298 K relative to S = 1 separated reactants. $\Delta G^{VTS} = \Delta G^{\ddagger} + \Delta_{Tun}$ = free energy barrier including tunneling effects at the VTS when using CHE-h_{10}. $\Delta G^{\ddagger} + \Delta_{Tun} + \Delta_{Deu}$ = free energy barrier when using CHE-d_{10}. [b]Includes correction for standard state change[32] and the substrate symmetry number[33] (see the SI). [c]The transition state point is changed to the VTS, and the corresponding energy change is included. [d]Includes tunneling effects (if any) in the reaction with CHE-d_{10}. [e]Predicted KIE value including all effects.

shown in Table 1 ($\Delta G^{\ddagger}$), $f_{SI}{}^{\circ}$ will become 1.0 for both **1** and **2** due to the favorable barriers of the S = 2 reactions. Hence, the reaction would occur in the high-spin state with certainty. We now define the fraction of S = 2 OAT products out of the total amount of S = 2 products as ^5f_O (eq 3), which is also given by the Boltzmann distribution function (the corresponding fraction ^3f_O for the S = 1 reactions is also defined in the same way)

$$ {}^5f_O = \frac{[{}^5P_O]}{[{}^5P_{tot}]} = \frac{e^{-{}^5\Delta G^{VTS(O)}/RT}}{e^{-{}^5\Delta G^{VTS(H)}/RT} + e^{-{}^5\Delta G^{VTS(O)}/RT}} \quad (3) $$

Using the values shown in Table 1 ($\Delta G^{\ddagger}$), ^5f_O will become 0.48 and 0.26 for **1** and **2**, respectively. These values therefore predict that all of the reactions occur in the high-spin state ($f_{SI}{}^{\circ}$ = 1), and a significant part of the products would be OAT products (^5f_O = 0.48 and 0.26 for **1** and **2**, respectively). Because no OAT products are seen in the experiments, we took the extra step of finding variational transition states (VTSs) for more accurate rates and evaluated tunneling corrections that should lower the HAT barriers, as suggested by the high experimental KIE. These results show that even with tunneling and VTSs (Table 1, $\Delta G^{\ddagger} + \Delta_{Tun}$), the amount of OAT products would have been appreciable ($f_{SI}{}^{\circ} \geq 0.84$ and $^5f_O \geq 0.16$, Table 2). Furthermore, the calculated KIEs of 4 and 5 for the S = 2 HAT (see Table 1) *are ten times lower than experimental values*, while the S = 1 HAT values are much closer to the experimental ones (>50). It is therefore clear that the S = 2 pathways are not optimally explored in the reaction. While it is always possible to invoke calculation errors, we show below that inclusion of SIP makes these results quite reasonable.

Thus, we define the real fraction of the total amount of products produced through the S = 2 state (f_{SI}) as follows (eq 4), which should be the same as the SIP:

$$ [{}^5P_{tot}] = f_{SI}[P_{tot}] \Leftrightarrow f_{SI} = \frac{[{}^5P_{tot}]}{[P_{tot}]} \quad (4) $$

In the above definition, the SIP may assume any value between, *and including*, 0 and 1. Hence, the equations derived below can be used regardless if there is TSR or not. This definition includes *all* of the possible effects that can affect the probability,

Table 2. Calculated Properties for Reactions of 1 and 2 with CHE-h_{10} and CHE-d_{10} at 298 K Including Tunneling

	1		2	
parameter	CHE-h_{10}	CHE-d_{10}	CHE-h_{10}	CHE-d_{10}
$[P_O]/[P_{tot}]$ (exp)	<0.01	0.20	<0.01	0.17
^3f_O	0.00	0.00	0.00	0.00
^5f_O	0.34	0.69	0.16	0.49
$f_{SI}{}^{\circ}$	0.84	0.99	1.00	1.00
f_{SI}	0.03	0.30	0.06	0.34
a	0.97	0.70	0.94	0.66
b	0.02	0.09	0.05	0.17
c	0.00	0.00	0.00	0.00
d	0.01	0.20	0.01	0.17
$k_2^{(app,tot,f_{SI}^{\circ})}$ (M^{-1} s^{-1})	2.3×10^{-2}	9.7×10^{-3}	2.5×10^{2}	8.4×10
$k_2^{(app,tot,f_{SI})}$ (M^{-1} s^{-1})	3.8×10^{-3}	9.8×10^{-5}	4.1×10^{-2}	8.7×10^{-4}
k_2 (M^{-1} s^{-1}) (exp)	4.5×10^{-2}	8.2×10^{-4}	4.5×10^{-1}	6.4×10^{-3}
KIE	39		47	
KIE (exp)	55(5)		66(5)	

such as the Boltzmann distributions of the different reactions (i.e., $f_{SI}{}^{\circ}$), SOC, minimum-energy crossing point (MECP) location, and other unspecified effects. Substitution of $[{}^5P_{tot}]$ in eq 3 into eq 4 yields

$$ f_{SI} = \frac{([{}^5P_O]/[P_{tot}])}{{}^5f_O} \approx \frac{([P_O]/[P_{tot}])}{{}^5f_O} \quad (5) $$

In the last part, we have used the fact that $[P_O] = [{}^3P_O] + [{}^5P_O]$ and that $[{}^3P_O] = 0$ due to very high- energy barriers (Table 1; see also the SI for a more general treatment). Hence, what eq 5 states is that given the measured fraction of the OAT products out of the total product yield ($[P_O]/[P_{tot}]$), we can calculate f_{SI}, which so far has been available only through painstaking ab initio calculations and not from experiments. The accuracy of f_{SI} will be limited only by the accuracy of the calculated ^5f_O and the measured $[P_O]/[P_{tot}]$ but not from the theory derived in this study as the equations are virtually free of approximations.

Table 2 shows the value of f_{SI} (including tunneling, calculated through eq 5) as 0.03 for **1** and 0.06 for **2**, as well as the fractions of the total product yield produced through each of the four pathways (a–d; see Figure 3 for the definition and the SI, Table S2 for formulas). As a result of the small f_{SI} for the CHE-h_{10} reaction, combined with the prohibitively large barrier for S = 1 OAT, nearly all of the reactions transpire through the S = 1 HAT pathway (a = 0.97 and 0.94 for **1** and **2**,

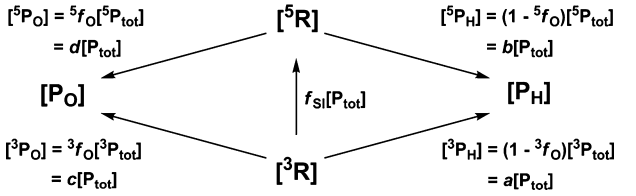

Figure 3. Four reaction pathways leading to HAT (P_H) and OAT (P_O) products from the ground-state reactant ^3R. f_O is the fraction of the OAT products formed in S = 1 or 2, and f_{SI} is the fraction of the total amount of products formed through the S = 2 state. a, b, c, and d are the fractions of the total amount of products. Many equations can now be derived from this picture, such as $a + b + c + d = 1$ and $b + d = f_{SI}$.

DOI: 10.1021/acs.jpclett.5b00527
J. Phys. Chem. Lett. 2015, 6, 1472−1476

respectively). This is consistent with the facts that (a) epoxidation products of CHE-h_{10} are not detected experimentally and (b) recent results that an oxidant with an $S = 2$ ground state performs epoxidation.[34]

We can now also provide a reason for observing OAT products only upon deuteration (vide supra). Deuteration should broaden the shape of the potential energy curve along the mass-scaled reaction coordinate while not affecting the electronic energy. This should make tunneling less efficient, and indeed, we see qualitatively a numerical cancellation of the tunneling effects when we calculate the CHE-d_{10} reaction barriers (Table 1, Δ_{Tun} versus Δ_{Deu} column). The deuteration, therefore, effectively raises the $S = 1$ HAT barrier, rendering the $S = 2$ pathways competitive and hence increasing f_{SI} to around 0.3 (Table 2). This shows that the role of tunneling is to effectively exclude $S = 2$ reactivity and, hence, eliminate any possibility for OAT products. We also note that because the calculated $S = 1$ OAT barrier is very high, the existence of OAT products is proof that the OAT reaction occurs through $S = 2$ by means of TSR. SIP should therefore be seriously considered in these types of reactions.

Because the calculated MECP is located before the transition state (see SI, Table S10), the SIP is mainly influenced by only two factors, the SOC and the $S = 2$ energy barrier heights in comparison to those on $S = 1$. Therefore, if we subtract out the effect of the latter one, that is, ${}^5\Delta G^{VTS}(f_{SI}) - {}^5\Delta G^{VTS}(f_{SI}{}^\circ)$, we will qualitatively obtain the influence of SOC. In the $S = 2$ CHE-d_{10} reactions, these differences are 3.4 and 7.4 kcal mol^{-1} for **1** and **2**, respectively. Hence, this procedure describes in principle a combined experimental and theoretical way to obtain a very crude estimate of the effect of SOC for **1** and **2** in terms of energy, assuming that there are no other major contributors to SIP than SOC.

The proportionality coefficients a–d allow us to obtain the apparent rate constant $k_2^{(app,tot,f_{SI})}$ of the overall reaction (see SI, Table S2 for formulas and values) and the KIE. The term "apparent" refers to the rate constant that would correspond to the observed amount of products. The KIE including multidimensional tunneling has recently been used as a powerful probe for the TSR.[35] The theoretically obtained KIEs are 39 for **1** and 47 for **2**, within acceptable error margins versus the experimental values. The rate constant values themselves are about a factor 10 off of the experimentally measured rates (Table S2, SI, corresponding to 1.4 kcal mol^{-1} in terms of energies at room temperature). We can compare these rate constants with what we would have without taking into account the experimental results, that is, $k_2^{(app,tot,f_{SI}{}^\circ)}$ (Table 2). In two of four cases, the use of f_{SI} significantly improves the agreement with experiments compared to the use of $f_{SI}{}^\circ$, while in only one case, the agreement is worse. This overall improvement in agreement with experiments is however not surprising considering that f_{SI} is partly determined by experiments in the first place; hence, it is important to remember here that the main parameter to be determined in this scheme is f_{SI} and not the rates. Therefore, the accuracy of the calculations and experiments mainly affects the accuracy of f_{SI}, but the model is robust enough to show consistency to experiments in terms of calculated rates.

Summarizing the results discussed above, we have presented arguments for considering both tunneling and SIP in a seemingly simple HAT reaction. We present a method to extract the SIP value of the reaction, which is normally difficult to obtain for these large systems, both experimentally and theoretically. To this end, we use CHE-h_{10} as the substrate. The intrinsic $S = 1$ HAT barrier is so high that at first glance, it would not seem to be a viable pathway. Tunneling effects downsize this barrier, and in conjunction with a low SIP, the use of the energetically more preferable $S = 2$ pathway is bypassed. When the tunneling effect is quantitatively quenched by substrate deuteration (CHE-d_{10}), the SIP is raised due to relatively more favorable $S = 2$ energies, and some OAT products are consequently seen. This effectively corroborates the TSR hypothesis as only a spin inversion could have produced OAT products, but the efficiency of this will depend on the SIP value. Attempts to calculate SOC and SIP's influence on FeO^+ species have previously been made,[35] and statistical arguments predicted low SIP on nonheme $Fe^{IV}O$ species.[36] The current examples highlight the role of TSR,[1,2] tunneling, deuteration and SIP, and the SIP determination by coupling experimental and theoretical data.

■ ASSOCIATED CONTENT

Supporting Information

Experimental and theoretical sections, including information on the materials and instrumentation used, generation and reactivity of $[(N4Py)Fe^{IV}O]^{2+}$ (**1**) and $[(Bn\text{-}TPEN)Fe^{IV}O]^{2+}$ (**2**), product analysis, styrene reactions, rate calculations, formulas used, and DFT details and coordinates. This material is available free of charge via the Internet at http://pubs.acs.org.

■ AUTHOR INFORMATION

Corresponding Authors

*E-mail: wwnam@ewha.ac.kr (W.N.).
*E-mail: sason@yfaat.ch.huji.ac.il (S.S.).
*E-mail: workforkyung@ewha.ac.kr (K.-B.C.).
*E-mail: yhkim@khu.ac.kr (Y.K.).

Author Contributions

#Y.H.K. and B.K.M. contributed equally to this study.

Notes

The authors declare no competing financial interest.

■ ACKNOWLEDGMENTS

The authors acknowledge the NRF of Korea through CRI (NRF-2012R1A3A2048842 to W.N.), MSIP (2013R1A1A2062737 to K.-B.C.), GRL (NRF-2010-00353 to W.N.), and KRF (NRF 2010-0012990 to Y.K.). S.S acknowledges the Israel Science Foundation (ISF Grant 1183/12).

■ REFERENCES

(1) Fiedler, A.; Schröder, D.; Shaik, S.; Schwarz, H. Electronic Structures and Gas-Phase Reactivities of Cationic Late-Transition-Metal Oxides. *J. Am. Chem. Soc.* **1994**, *116*, 10734–10741.

(2) Shaik, S.; Danovich, D.; Fiedler, A.; Schröder, D.; Schwarz, H. Two-State Reactivity in Organometallic Gas-Phase Ion Chemistry. *Helv. Chim. Acta* **1995**, *78*, 1393–1407.

(3) Kumar, D.; Hirao, H.; Que, L., Jr.; Shaik, S. Theoretical Investigation of C–H Hydroxylation by $(N4Py)Fe^{IV}O^{2+}$: An Oxidant More Powerful than P450? *J. Am. Chem. Soc.* **2005**, *127*, 8026–8027.

(4) Comba, P. Oxidation Catalysis with High-Valent Nonheme Iron Complexes. In *Molecular Catalysts: Structure and Functional Design*; Gade, L. H., Hofmann, P., Eds.; Wiley-VCH Verlag GmbH & Co. KGaA: Weinheim, Germany, 2014; pp 123–146.

(5) Hohenberger, J.; Ray, K.; Meyer, K. The Biology and Chemistry of High-Valent Iron-Oxo and Iron-Nitrido Complexes. *Nat. Commun.* **2012**, *3*, 720 DOI: 10.1038/ncomms1718.

DOI: 10.1021/acs.jpclett.5b00527
J. Phys. Chem. Lett. 2015, 6, 1472–1476

(6) Ye, S.; Neese, F. Quantum Chemical Studies of C−H Activation Reactions by High-Valent Nonheme Iron Centers. *Curr. Opin. Chem. Biol.* **2009**, *13*, 89−98.
(7) Usharani, D.; Janardanan, D.; Li, C.; Shaik, S. A Theory for Bioinorganic Chemical Reactivity of Oxometal Complexes and Analogous Oxidants: The Exchange and Orbital-Selection Rules. *Acc. Chem. Res.* **2013**, *46*, 471−482.
(8) Kazaryan, A.; Baerends, E. J. Ligand Field Effects and the High Spin−High Reactivity Correlation in the H Abstraction by Non-Heme Iron(IV)−Oxo Complexes: A DFT Frontier Orbital Perspective. *ACS Catal.* **2015**, *5*, 1475−1488.
(9) Sastri, C. V.; Lee, J.; Oh, K.; Lee, Y. J.; Lee, J.; Jackson, T. A.; Ray, K.; Hirao, H.; Shin, W.; Halfen, J. A.; et al. Axial Ligand Tuning of a Nonheme Iron(IV)−Oxo Unit for Hydrogen Atom Abstraction. *Proc. Natl. Acad. Sci. U.S.A.* **2007**, *104*, 19181−19186.
(10) Kuppermann, A.; Truhlar, D. G. Exact Tunneling Calculations. *J. Am. Chem. Soc.* **1971**, *93*, 1840−1851.
(11) Maity, D. K.; Bell, R. L.; Truong, T. N. Mechanism and Quantum Mechanical Tunneling Effects on Inner Hydrogen Atom Transfer in Free Base Porphyrin: A Direct Ab Initio Dynamics Study. *J. Am. Chem. Soc.* **2000**, *122*, 897−906.
(12) Zhang, F.; Dibble, T. S. Impact of Tunneling on Hydrogen-Migration of the N-Propylperoxy Radical. *Phys. Chem. Chem. Phys.* **2011**, *13*, 17969−17977.
(13) Dybala-Defratyka, A.; Paneth, P.; Banerjee, R.; Truhlar, D. G. Coupling of Hydrogenic Tunneling to Active-Site Motion in the Hydrogen Radical Transfer Catalyzed by a Coenzyme B_{12}-Dependent Mutase. *Proc. Natl. Acad. Sci. U.S.A.* **2007**, *104*, 10774−10779.
(14) Klippenstein, S. J.; Pande, V. S.; Truhlar, D. G. Chemical Kinetics and Mechanisms of Complex Systems: A Perspective on Recent Theoretical Advances. *J. Am. Chem. Soc.* **2013**, *136*, 528−546.
(15) Truhlar, D. G.; Gao, J.; Alhambra, C.; Garcia-Viloca, M.; Corchado, J.; Sánchez, M. L.; Villà, J. The Incorporation of Quantum Effects in Enzyme Kinetics Modeling. *Acc. Chem. Res.* **2002**, *35*, 341−349.
(16) Zuev, P. S.; Sheridan, R. S.; Albu, T. V.; Truhlar, D. G.; Hrovat, D. A.; Borden, W. T. Carbon Tunneling from a Single Quantum State. *Science* **2003**, *299*, 867−870.
(17) Mai, B. K.; Kim, Y. Theoretical Studies for Large Tunneling and the Hydrogen-Transfer Mechanism in the C-H Activation of CH_3CN by a Di(μ-oxo)Diiron(IV) Complex: A Model for Intermediate Q in Soluble Methane Monooxygenase. *Chem.—Eur. J.* **2013**, *19*, 3568−3572.
(18) Hu, S.; Sharma, S. C.; Scouras, A. D.; Soudackov, A. V.; Carr, C. A. M.; Hammes-Schiffer, S.; Alber, T.; Klinman, J. P. Extremely Elevated Room-Temperature Kinetic Isotope Effects Quantify the Critical Role of Barrier Width in Enzymatic C−H Activation. *J. Am. Chem. Soc.* **2014**, *136*, 8157−8160.
(19) Park, K.; Pak, Y.; Kim, Y. Large Tunneling Effect on the Hydrogen Transfer in Bis(μ-Oxo)Dicopper Enzyme: A Theoretical Study. *J. Am. Chem. Soc.* **2012**, *134*, 3524−3531.
(20) Mandal, D.; Ramanan, R.; Usharani, D.; Janardanan, D.; Wang, B.; Shaik, S. How Does Tunneling Contribute to Counterintuitive C−H Abstraction Reactivity of Nonheme Fe(IV)O Oxidants with Alkanes? *J. Am. Chem. Soc.* **2015**, *137*, 722−733.
(21) Schreiner, P. R.; Reisenauer, H. P.; Ley, D.; Gerbig, D.; Wu, C.-H.; Allen, W. D. Methylhydroxycarbene: Tunneling Control of a Chemical Reaction. *Science* **2011**, *332*, 1300−1303.
(22) Oloo, W. N.; Feng, Y.; Iyer, S.; Parmelee, S.; Xue, G.; Que, L., Jr. Cyclohexene as a Substrate Probe for the Nature of the High-Valent Iron-Oxo Oxidant in Fe(TPA)-Catalyzed Oxidations. *New J. Chem.* **2013**, *37*, 3411−3415.
(23) In iron porphyrin systems (e.g., oxoiron(IV) porphyrin π-cation radical species), cyclohexene oxide was obtained as the major product at room temperature; see refs 24−26.
(24) Takahashi, A.; Kurahashi, T.; Fujii, H. Activation Parameters for Cyclohexene Oxygenation by an Oxoiron(IV) Porphyrin π-Cation Radical Complex: Entropy Control of an Allylic Hydroxylation Reaction. *Inorg. Chem.* **2007**, *46*, 6227−6229.
(25) Song, W.; Ryu, Y.; Song, R.; Nam, W. Oxoiron(IV) Porphyrin π-Cation Radical Complexes with a Chameleon Behavior in Cytochrome P450 Model Reactions. *J. Biol. Inorg. Chem.* **2005**, *10*, 294−304.
(26) Groves, J.; Gross, Z. On the Mechanism of Epoxidation and Hydroxylation Catalyzed by Iron Porphyrins. Evidence for Non-Intersecting Reaction Pathways. In *Bioinorganic Chemistry: An Inorganic Perspective of Life*; Kessissoglou, D. P., Ed.; NATO ASI Series; Springer: Amsterdam, The Netherlands, 1995; Vol. *459*, pp 39−47.
(27) Cho, K.-B.; Wu, X.; Lee, Y.-M.; Kwon, Y. H.; Shaik, S.; Nam, W. Evidence for an Alternative to the Oxygen Rebound Mechanism in C−H Bond Activation by Non-Heme $Fe^{IV}O$ Complexes. *J. Am. Chem. Soc.* **2012**, *134*, 20222−20225.
(28) Company, A.; Prat, I.; Frisch, J. R.; Mas-Ballesté, D. R.; Güell, M.; Juhász, G.; Ribas, X.; Münck, D. E.; Luis, J. M.; Que, L., Jr.; Costas, M. Modeling the Cis-Oxo-Labile Binding Site Motif of Non-Heme Iron Oxygenases: Water Exchange and Oxidation Reactivity of a Non-Heme Iron(IV)-Oxo Compound Bearing a Tripodal Tetradentate Ligand. *Chem.—Eur. J.* **2011**, *17*, 1622−1634.
(29) Parsell, T. H.; Behan, R. K.; Green, M. T.; Hendrich, M. P.; Borovik, A. S. Preparation and Properties of a Monomeric Mn^{IV}−Oxo Complex. *J. Am. Chem. Soc.* **2006**, *128*, 8728−8729.
(30) Truhlar, D. G.; Garrett, B. C. Variational Transition State Theory. *Annu. Rev. Phys. Chem.* **1984**, *35*, 159−189.
(31) Miwa, G. T.; Lu, A. Y. H. Kinetic Isotope Effects and "Metabolic Switching" in Cytochrome P450-Catalyzed Reactions. *BioEssays* **1987**, *7*, 215−219.
(32) Winget, P.; Cramer, C. J.; Truhlar, D. G. Computation of Equilibrium Oxidation and Reduction Potentials for Reversible and Dissociative Electron-Transfer Reactions in Solution. *Theor. Chem. Acc.* **2004**, *112*, 217−227.
(33) Benson, S. W. Statistical Factors in the Correlation of Rate Constants and Equilibrium Constants. *J. Am. Chem. Soc.* **1958**, *80*, 5151−5154.
(34) Biswas, A. N.; Puri, M.; Meier, K. K.; Oloo, W. N.; Rohde, G. T.; Bominaar, E. L.; Münck, E.; Que, L., Jr. Modeling TauD-*J*: A High-Spin Nonheme Oxoiron(IV) Complex with High Reactivity toward C−H Bonds. *J. Am. Chem. Soc.* **2015**, *137*, 2428−2431.
(35) Mai, B. K.; Kim, Y. The Kinetic Isotope Effect as a Probe of Spin Crossover in the C−H Activation of Methane by the FeO^+ Cation. *Angew. Chem., Int. Ed.* **2015**, *54*, 3946−3951.
(36) Cho, K.-B.; Kim, E. J.; Seo, M. S.; Shaik, S.; Nam, W. Correlating DFT-Calculated Energy Barriers to Experiments in Nonheme Octahedral $Fe^{IV}O$ Species. *Chem.—Eur. J.* **2012**, *18*, 10444−10453.

DOI: 10.1021/acs.jpclett.5b00527
J. Phys. Chem. Lett. 2015, 6, 1472−1476